Tau antagonizes end-binding protein tracking at microtubule ends through a phosphorylation- dependent mechanism

Sacnicte Ramirez-Rios, Eric Denarier, Elea Prezel, Angélique Vinit, Virginie Stoppin-Mellet, François Devred, Pascale Barbier, Vincent Peyrot, Carmen Laura Sayas, Jesús Avila, et al.

Tau antagonizes end-binding protein tracking at microtubule ends through a phosphorylation-dependent mechanism

Sacnicte Ramirez-Rios[a,b], Eric Denarier[a,b,c], Eléa Prezel[a,b,†], Angélique Vinit[a,b,†], Virginie Stoppin-Mellet[a,b], François Devred[d], Pascale Barbier[d], Vincent Peyrot[d], Carmen Laura Sayas[e], Jesus Avila[f], Leticia Peris[a,b], Annie Andrieux[a,b,c], Laurence Serre[a,b], Anne Fourest-Lieuvin[a,b,c], and Isabelle Arnal[a,b,*]

[a]Université Grenoble Alpes, Grenoble Institut des Neurosciences, F-38000 Grenoble, France; [b]INSERM, U1216, F-38000 Grenoble, France; [c]CEA, BIG-GPC, F-38000 Grenoble France; [d]Aix-Marseille Université, INSERM, CRO2 UMR_S 911, Faculté de Pharmacie, F-13385 Marseille, France; [e]Centro de Investigaciones Biomédicas de Canarias entro de Investigaciones Biomédicas de Canarias, Instituto de Tecnologías Biomédicas, Universidad de La Laguna, 38071 Tenerife, Spain; [f]Centro de Biología Molecular "Severo Ochoa" (CSIC-UAM), 28029 Madrid, Spain

ABSTRACT Proper regulation of microtubule dynamics is essential for cell functions and involves various microtubule-associated proteins (MAPs). Among them, end-binding proteins (EBs) accumulate at microtubule plus ends, whereas structural MAPs bind along the microtubule lattice. Recent data indicate that the structural MAP tau modulates EB subcellular localization in neurons. However, the molecular determinants of EB/tau interaction remain unknown, as is the effect of this interplay on microtubule dynamics. Here we investigate the mechanisms governing EB/tau interaction in cell-free systems and cellular models. We find that tau inhibits EB tracking at microtubule ends. Tau and EBs form a complex via the C-terminal region of EBs and the microtubule-binding sites of tau. These two domains are required for the inhibitory activity of tau on EB localization to microtubule ends. Moreover, the phosphomimetic mutation S262E within tau microtubule-binding sites impairs EB/tau interaction and prevents the inhibitory effect of tau on EB comets. We further show that microtubule dynamic parameters vary, depending on the combined activities of EBs and tau proteins. Overall our results demonstrate that tau directly antagonizes EB function through a phosphorylation-dependent mechanism. This study highlights a novel role for tau in EB regulation, which might be impaired in neurodegenerative disorders.

INTRODUCTION

Microtubules are major components of the eukaryotic cytoskeleton and are essential for intracellular transport, mitosis, and cellular architecture (Desai and Mitchison, 1997). They are 25-nm hollow cylinders resulting from the assembly of α/β-tubulin heterodimers (Amos and Schlieper, 2005). Microtubule ends constantly oscillate between phases of polymerization and depolymerization, a behavior known as dynamic instability (Mitchison and Kirschner, 1984). Transitions from growth to shortening are referred to as catastrophes and reverse events as rescues. In living cells, a variety of microtubule-associated proteins (MAPs) interact with free tubulin and/or microtubules to regulate their properties and spatial organization. Plus end– tracking proteins (+TIPs) are a diverse group of MAPs that preferentially associate with the growing plus ends of microtubules (Galjart, 2010). The +TIPs form a complex interaction network at microtubule plus ends, where they control both microtubule dynamics and microtubule anchorage to distinct subcellular targets (e.g., cell cortex, vesicles, kinetochores).

Supplemental Material can be found at:
http://www.molbiolcell.org/content/suppl/2016/07/25/mbc.E16-01-0029v1.DC1.html
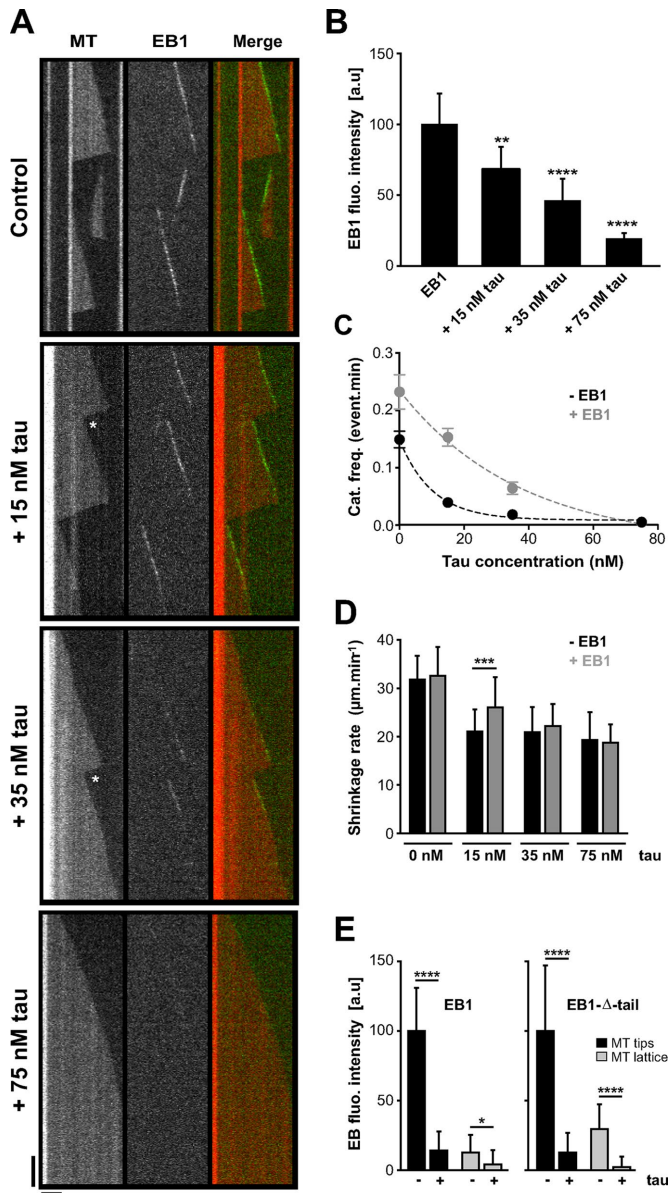
FIGURE 1: Tau inhibits EB1 tracking at microtubule ends in a concentration-dependent manner. (A) Kymographs of microtubules assembled in the presence of 75 nM GFP-EB1 alone or with combinations of 75 nM GFP-EB1 and increasing concentrations of tau (15, 35, and 75 nM). The white stars indicate rescues after catastrophe events. Horizontal and vertical bars, 5 μm and 60 s, respectively. MT, microtubule. (B) Histogram indicating GFP-EB1 fluorescence intensity at microtubule tips in the absence or presence of increasing tau concentration. ** $p < 0.01$, **** $p < 0.0001$ (Kruskal–Wallis analysis of variance [ANOVA] followed by post hoc Dunn's comparison; $n = 35$, 75, 81, and 34 for GFP-EB1, GFP-EB1 + 15 nM tau, GFP-EB1 + 35 nM tau, and GFP-EB1 + 75 nM tau, respectively). The p values were calculated in comparison to the condition without tau. a.u., arbitrary units. (C) Catastrophe frequency vs. tau concentration in the absence (black) or presence (gray) of GFP-EB1. Data were fitted by a one-phase exponential decay model ($R^2 = 0.99$ for both data sets), and the two curves were significantly different with $p = 0.02$ (F-test). (D) Microtubule shrinkage rates measured with or without GFP-EB1 (75 nM) and at increasing tau concentrations (0, 15, 35, and 75 nM). *** $p < 0.001$ (Mann–Whitney U test, $n = 22$ and 104 for tau 15 nM and tau 15 nM + GFP-EB1, respectively). (E) Histograms showing GFP-EB1 (left) and GFP-EB1-Δ-tail (right) fluorescence intensity at microtubule tips and on the microtubule lattice in the presence or absence of

Among the +TIP family, end-binding protein 1 (EB1) is considered as a major integrator of microtubule end behavior (Akhmanova and Steinmetz, 2010). EB1 autonomously end-tracks growing microtubules, where it recruits many other +TIPs, ensuring tight control of microtubule properties (Bieling *et al.*, 2007; Dixit *et al.*, 2009; Honnappa *et al.*, 2009; Zanic *et al.*, 2009; Zimniak *et al.*, 2009). EB1 and its homologues (EB2 and 3) in mammals are composed of an N-terminal calponin-homology domain, which is required for microtubule binding, and a C-terminal dimerization domain (Hayashi and Ikura, 2003; Honnappa *et al.*, 2005; Slep *et al.*, 2005; De Groot *et al.*, 2010). The C-terminal part includes a unique EB1 homology (EBH) domain followed by an acidic C-terminal tail, both of which are involved in the interactions of EBs with multiple partners (Akhmanova and Steinmetz, 2010). Because of its central role in the +TIP network, the association of EB1 with microtubule ends is tightly regulated to ensure precise spatiotemporal control of the cytoskeleton. The mechanisms underlying this regulation, however, are poorly understood.

Recent studies have proposed that the localization of EB proteins (EB1 and 3) on microtubules is modulated by structural MAPs primarily characterized by their binding along the microtubule lattice (Kapitein *et al.*, 2011; Sayas and Avila, 2014; Velot *et al.*, 2015). Examples of this cross-talk include MAP2-dependent distribution of EB3 along dendritic microtubules upon neuronal activation (Kapitein *et al.*, 2011) and sequestration of EB1/3 by MAP1B in the cytosol of neuronal cells (Tortosa *et al.*, 2013). Tau is another major structural MAP involved in the neuronal development and maintenance of the brain integrity. We recently identified tau as a partner of EBs in neurons and found that tau regulates EB subcellular localization (Sayas *et al.*, 2015). The molecular basis of such interplay and the consequences for microtubule dynamic behavior are unknown.

Here we sought to dissect how tau and its phosphorylation affect EB behavior at microtubule tips. We provide biochemical and cell-biological evidence that tau inhibits the microtubule-end tracking properties of EBs. We find that the basic microtubule-binding sites of tau directly interact with the C-terminal region of EBs and that these two interacting domains are required for the inhibitory activity of tau on EB localization to microtubule ends. Of note, a phosphomimetic mutation S262E within tau microtubule-binding sites impairs EB/tau interaction. This S262E-tau mutant does not inhibit the formation of EB comets. Our results further show that the parameters of microtubule dynamics change depending on the combined activities of EB and tau proteins. Taken together, our data support a novel mechanism by which tau directly regulates EB properties at microtubule ends.

RESULTS

Tau inhibits EB1 tracking at microtubule plus ends

We investigated whether tau affected EB1 intrinsic properties by reconstituting in vitro microtubule dynamics and EB1 tracking at microtubule ends using total internal reflection fluorescence (TIRF) microscopy (Figure 1A). Red-labeled purified tubulin was nucleated from brightly fluorescent seeds, and microtubule behavior was analyzed in the presence of green fluorescent protein (GFP)–EB1, tau, and combinations of the two proteins. In the control conditions (tubulin alone), microtubules alternated between phases of growth and shortening (Table 1). GFP-EB1 formed comets at the extremity

---

tau. Equimolar concentrations (75 nM) of GFP-EB1, GFP-EB1-Δ-tail, and tau were used. * $p < 0.05$, **** $p < 0.0001$ (Mann–Whitney U test comparison, $n = 20$ for each condition). All error bars represent SDs.

	Growth rate (μm/min)	Shortening rate (μm/min)	Catastrophe frequency (events/min)	Rescue frequency (events/min)
Control	1.53 ± 0.25 n = 119	31.78 ± 4.73 n = 102	0.149 ± 0.014 n = 103	0
GFP-EB1 (75 nM)	1.91 ± 0.33 n = 59	32.66 ± 5.62 n = 56	0.232 ± 0.031 n = 56	0
tau (15 nM)	1.75 ± 0.28 n = 54	21.09 ± 4.36 n = 22	0.039 ± 0.008 n = 20	1.66 ± 0.35 n = 22
tau (35 nM)	1.70 ± 0.27 n = 45	20.92 ± 4.99 n = 12	0.018 ± 0.005 n = 12	1.21 ± 0.38 n = 10
tau (75 nM)	2.06 ± 0.27 n = 51	19.32 ± 5.52 n = 4	0.005 ± 0.0025 n = 4	1.58 ± 0.79 n = 4
GFP-EB1 + 15 nM tau	1.88 ± 0.35 n = 125	26.01 ± 6.09 n = 104	0.153 ± 0.015 n = 97	1.75 ± 0.20 n = 73
GFP-EB1 + 35 nM tau	1.76 ± 0.34 n = 64	22.18 ± 4.35 n = 37	0.064 ± 0.010 n = 37	2.61 ± 0.43 n = 36
GFP-EB1 + 75 nM tau	1.93 ± 0.23 n = 42	18.73 ± 3.59 n = 4	0.004 ± 0.002 n = 4	1.36 ± 0.68 n = 4

Dynamic parameters were measured for microtubules assembled with tubulin (12 μM) in the absence or presence of the indicated proteins. The total times of measurements (growing and shrinkage phases) were 723.80, 261.92, 514.74, 666.96, 742.74, 674.38, 583.67, and 850.78 min for tubulin alone, 75 nM GFP-EB1, 15 nM tau, 35 nM tau, 75 nM tau, 75 nM GFP-EB1 + 15 nM tau, 75 nM GFP-EB1 + 35 nM tau, and 75 nM GFP-EB1 + 75 nM tau, respectively. n, number of events measured for each condition. Values represent mean ± SD.

TABLE 1: Effects of EB1 and tau on microtubule dynamics.

of growing microtubules (Figure 1, A and B) and stimulated catastrophes (Table 1 and Supplemental Movie S1), as reported previously (Bieling et al., 2007; Vitre et al., 2008; Komarova et al., 2009; Zanic et al., 2013). Conversely, tau strongly decreased the catastrophe frequency (from 0.149 event/min in the tubulin-alone control to 0.005 event/min with the highest tau concentration; Table 1), induced rescues, and slowed the microtubule shrinkage rate (Table 1). Such effects already could be observed at very low tau:tubulin ratios (15 nM tau; Table 1) and are consistent with the known microtubule-stabilizing properties of this neuronal MAP (Panda et al., 1995, 2003). Strikingly, the simultaneous addition of GFP-EB1 and tau reduced GFP-EB1 localization at microtubule ends in a tau concentration–dependent manner (Figure 1, A and B). Using a fixed amount of GFP-EB1 (75 nM) and increasing concentrations of tau (0, 15, 35, and 75 nM), we observed a gradual decrease in GFP-EB1 comet intensity from 100 a.u. in the absence of tau to 19 a.u with 75 nM tau (Figure 1B and Supplemental Movie S1). This progressive inhibition of GFP-EB1 end-tracking properties was accompanied by large changes in microtubule dynamics. In the presence of GFP-EB1 alone, microtubules were highly unstable, undergoing catastrophes without rescue events (i.e., total depolymerization of the polymer down to the seeds; Figure 1A and Table 1). On addition of 15 nM tau, a portion of the shrinking events was rescued before the total depolymerization of microtubules due to concomitant destabilizing and stabilizing activities of EB1 and tau, respectively. In contrast, microtubules assembled with equimolar amounts (75 nM) of GFP-EB1 and tau grew persistently with a catastrophe frequency as low as with tau alone, showing that EB1 effects on microtubule dynamics were hampered by tau in this condition.

We next wondered whether EB1 could reciprocally affect the microtubule-regulating properties of tau. We noticed that, at substoichiometric tau concentrations relative to GFP-EB1, the inhibitory activity of tau on catastrophes was affected by the presence of GFP-EB1 (Figure 1C). In particular, combination of 15 nM tau and 75 nM GFP-EB1 strongly altered the capacity of tau to reduce the catastrophe rate compared with 15 nM tau alone. At this low tau:EB1 ratio, microtubules also disassembled faster than with tau alone, indicating that they were less stabilized (Figure 1D). These results suggested that a fraction of tau might be prevented from binding to the microtubule wall in the presence of EB1. Moreover, cosedimentation assays revealed that an excess of EB1 could displace tau molecules bound to Taxol-stabilized microtubules (Supplemental Figure S1A and Supplemental Materials and Methods). In these conditions, a portion of EB1 associates with microtubules (Maurer et al., 2012; Zhang et al., 2015) and can compete with the microtubule-binding sites of tau. We thus produced a mutant of EB1 (EB1-KQ/EE) with impaired microtubule-binding properties by substituting K100 and Q102 in the CH domain with glutamate residues (Maurer et al., 2012; Zhang et al., 2015). EB1-KQ/EE still induced a significant release of tau from microtubules (Supplemental Figure S1B), supporting the hypothesis that soluble EB1 affects tau binding to the microtubule wall.

We then asked whether tau could recruit EB1 along the microtubule wall in our reconstitution assay, since EB proteins have been identified as partners of structural MAPs in neurons (Kapitein et al., 2011; Tortosa et al., 2013; Sayas et al., 2015; see later description). The very weak GFP-EB1 labeling observed along the microtubule lattice by TIRF microscopy was not enhanced in the presence of equimolar amount of tau (75 nM) and was even slightly reduced compared with GFP-EB1 alone (Figure 1E, left). To confirm this result, we produced a GFP-EB1 construct lacking the last 20 residues (GFP-EB1-Δ-tail) and exhibiting enhanced binding to the microtubule wall compared with full-length EB1 (Buey et al., 2011). The results showed that the intensity of GFP-EB1-Δ-tail decreased drastically both at microtubule ends and along the microtubule lattice in the presence of equimolar amount of tau (Figure 1E, right). Thus tau inhibits the binding of EB1 along the microtubule wall in vitro.
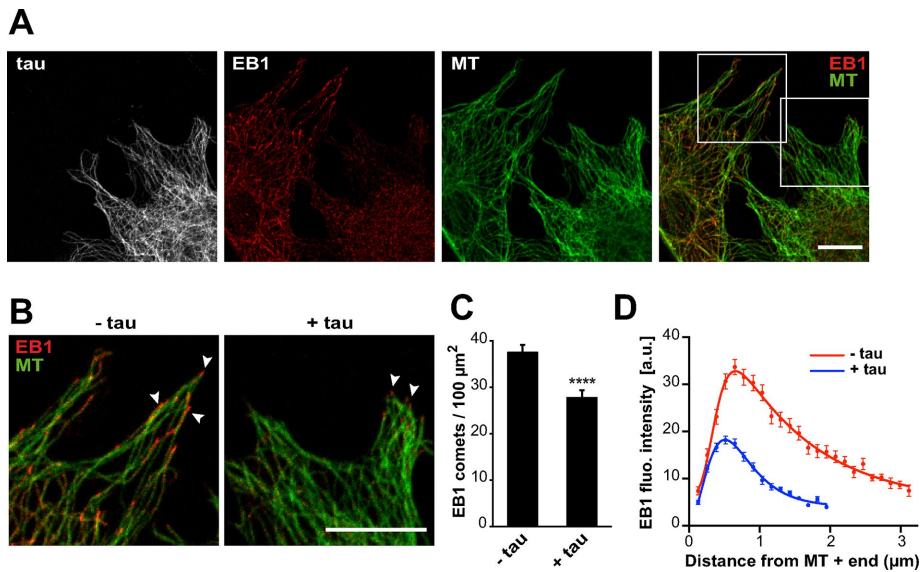
FIGURE 2: Tau inhibits EB localization at microtubule ends in fibroblasts. (A) Mouse embryonic fibroblasts were transfected with pEGFP-tau and stained for EGFP (tau, gray), EB1 (red), and tubulin (MT, green). Right, merged image with EB1 and tubulin staining. Images include transfected and nontransfected cells in the same field. Bar, 10 μm. (B) Higher magnifications of nontransfected (−tau) and transfected (+tau) cells. Arrowheads point to comets. Bar, 10 μm. (C) EB1 comet density normalized to the microtubule network surface (comet number/100 μm² of microtubule network) in lamellipodia of nontransfected (−tau) or pEGFP-tau transfected (+tau) cells. The histogram shows the mean ± SEM. ****$p < 0.0001$, Mann-Whitney U test comparison ($n = 80$ and 88 regions of interest for −tau and +tau conditions, respectively). (D) The fluorescence intensity of comets was quantified in nontransfected (−tau) and transfected (+tau) cells and plotted against the distance from microtubule plus ends. Nonlinear regression curves fitting the mean fluorescence intensities ± SEM (70 and 95 comets for −tau and +tau conditions, respectively). a.u., arbitrary units.

We next investigated whether tau affected EB behavior in a cellular model. Mouse embryonic fibroblasts, devoid of endogenous tau, were transfected with EGFP-tau and immunolabeled for EB1. In agreement with the results obtained with purified proteins, we observed a reduction of EB1 comets in cells expressing tau (Figure 2, A and B). Quantifications showed that both the density (Figure 2C) and mean intensity (Figure 2D) of comets were markedly decreased. Furthermore, the mean length of comets was reduced from 2.28 μm ± 0.06 (SEM, $n = 70$ comets) in nontransfected cells to 1.30 μm ± 0.03 ($n = 95$ comets) in tau-transfected cells. We also noticed relocation of EB1 along tau-induced microtubule bundles in some cells expressing high levels of tau (Supplemental Figure S2; see *Discussion*), as reported previously in neurons (Sayas *et al.*, 2015). Overall these results demonstrate that tau inhibits EB1 localization at microtubule ends.

Tau inhibitory effect on EB tracking at microtubule ends is mediated by the C-terminal part of EBs

The inhibitory effect of tau on EB1 end-tracking properties might rely on a direct interaction between tau and EB1. Accordingly, we recently identified tau as a partner of EB1 in neurons (Sayas *et al.*, 2015) and showed that EB1 directly binds tau in pull-down experiments using purified proteins (Figure 3A and Supplemental Figure S3A). To quantify this interaction, we estimated the apparent affinity of tau and EB1 by fluorescence spectroscopy (Supplemental Figure S3B). EB1 fluorescence upon tau addition showed saturable quenching, indicating the formation of a complex between the two proteins with an apparent dissociation constant of 1.7 ± 1.1 μM. We next determined the tau-interacting region in EB1. EBs consist of an

N-terminal domain responsible for microtubule binding and a C-terminal part involved in dimerization and interaction with many partners. We used the EB1-NL-LZ construct, in which the whole C-terminal part of EB1 was removed and replaced by the leucine zipper domain of yeast GCN4 to artificially dimerize the N-terminal domain of EB1 (Komarova *et al.*, 2009; Buey *et al.*, 2011). Pull-down experiments revealed that EB1-NL-LZ was far less efficient in binding tau than EB1 (Figure 3A), indicating that EB1 interacted with tau through its C-terminal domain. We then evaluated by TIRF microscopy whether the C-terminal part of EBs was also required for the inhibitory activity of tau on EB tracking at microtubule tips. For these experiments, EB3 appeared more suitable than EB1 since, in contrast with EB1, the removal of the C-terminal part of EB3 does not significantly affect its microtubule end–binding properties (Komarova *et al.*, 2009; Skube *et al.*, 2010; Buey *et al.*, 2011). We thus used the chimera GFP-EB3-NL-LZ, which accumulated at microtubule ends and promoted catastrophe events similar to GFP-EB3 (Figure 3B and Table 2; Komarova *et al.*, 2009; Buey *et al.*, 2011). Increasing concentrations of tau strongly decreased the comet intensity of GFP-EB3 (Figure 3, B and C, and Supplemental Movie S2), as observed earlier for GFP-EB1 (Figure 1).

Moreover, microtubules assembled with both GFP-EB3 and tau elongated with few catastrophes and some rescue events, showing that tau impeded the microtubule-destabilizing activity of EB3 (Table 2). By contrast, for equimolar concentrations of tau and GFP-EB3-NL-LZ, tau did not inhibit GFP-EB3-NL-LZ binding at microtubule ends (comet intensity of 109 a.u. with 10 nM tau versus 100 a.u. without tau), and we observed only a slight decrease of GFP-EB3-NL-LZ comet intensity at higher tau concentration (comet intensity of 68 a.u. with 40 nM tau compared with 100 a.u. without tau; Figure 3, B and D, and Supplemental Movie S3). In these conditions, microtubules were highly dynamic and exhibited both catastrophes and rescues due to the concomitant microtubule-regulating activities of GFP-EB3-NL-LZ and tau, respectively (Table 2). Taken together, these results reveal that the C-terminal region of EBs interacts with tau and is a key element for the inhibitory effect of tau on EB tracking at microtubule ends.

The basic microtubule-binding sites of tau directly interact with EB1

We next intended to determine the motifs of tau involved in EB1 binding. Tau can be divided into two main regions (Figure 4A): an acidic, N-terminal projection domain and a basic, C-terminal domain, which is composed of a proline-rich region (P2), four conserved basic repeats (R1–R4), and a C-terminal extension including a pseudorepeat (R'). The repeat motifs and flanking sequences (i.e., P2 and R') constitute the microtubule-binding domain (MTBD) and are responsible for the microtubule-stabilizing properties of tau (Trinczek *et al.*, 1995; Mukrasch *et al.*, 2007, 2009). The N-terminal part of tau contains one putative consensus EB binding site (TXIP;
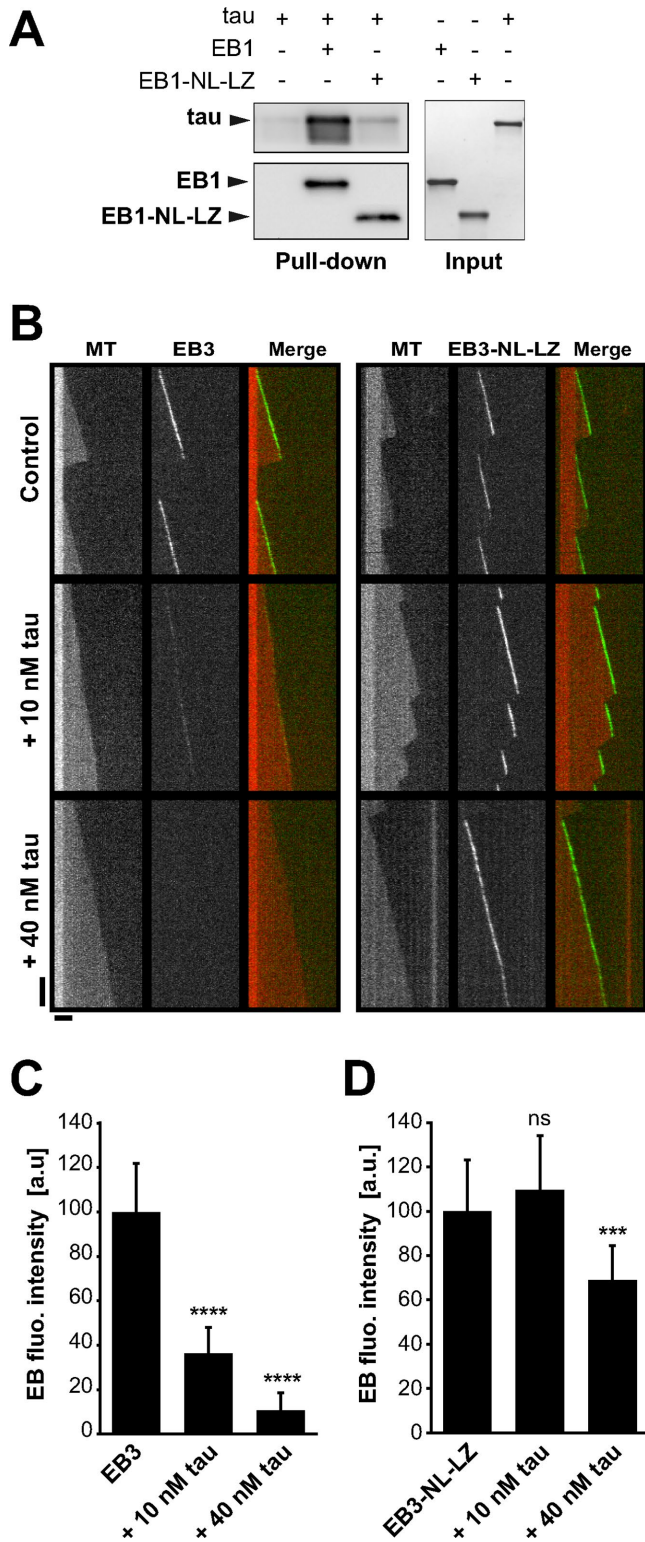
FIGURE 3: Tau inhibitory effect on microtubule-tracking properties of EBs requires the C-terminal part of EBs. (A) Pull-down assays of tau with biotinylated-EB1 or biotinylated-EB1-NL-LZ. (B) Kymographs of microtubules assembled with 10 nM GFP-EB3 (left) or GFP-EB3-NL-LZ (right) in the absence (control) or presence of increasing concentrations of tau. Protein concentrations were decreased compared with conditions with GFP-EB1 and tau (Figure 1) to avoid GFP-EB3-NL-LZ binding to the microtubule lattice. Horizontal and vertical bars, 5 μm and 60 s, respectively. MT, microtubule. (C, D) Fluorescence intensity of GFP-EB3 (C) and GFP-EB3-NL-LZ

Supplemental Figure S4A; Honnappa *et al.*, 2009). We performed several mutations to invalidate this site in the tau protein, but these mutations neither altered tau/EB1 interaction nor modified tau-dependent inhibition of EB1 comets (Supplemental Figure S4, B and C). We thus focused on the basic domains of tau, as they might interact with the negatively charged C-terminal part of EBs. We produced various forms of tau (Figure 4A): 0R-tau (deletion of the four repeats), R1R'-tau (tau fragment from R1 to R'), and P2R'-tau (tau fragment from P2 to R'). Removal of R1–R4 repeats (0R-tau) completely abolished tau interaction with EB1 (Figure 4B). EB1 still bound the two fragments R1R'- and P2R'-tau, however, indicating that the repeat motifs of tau are necessary for the formation of a complex between the two proteins. TIRF assays revealed that 0R-tau was not able to inhibit the tracking of GFP-EB1 at microtubule ends (Figure 4, C and D). This suggested that tau repeats were required for the inhibition of EB1 accumulation at microtubule ends. However, the minimal fragment R1R'-tau including the repeats only slightly decreased the comet intensity of GFP-EB1 compared with the full-length tau (68 vs. 8 a.u., respectively; Figure 4D). By contrast, the fragment of tau containing the P2 domain in addition to the repeat motifs (P2R'-tau fragment) strongly inhibited GFP-EB1 tracking at microtubule tips to the same extent as tau (7 and 8 a.u., respectively; Figure 4D). Overall these data indicate that the inhibitory activity of tau on EB comets requires both the microtubule-binding repeats and the P2 region of tau.

The interaction between tau and EB1 is regulated by phosphorylation

The microtubule-stabilizing properties of tau are tightly regulated by phosphorylation (Buee *et al.*, 2000). Given that EB1 interacts with the basic microtubule-binding sites of the neuronal MAP, phosphorylation in this region might affect tau/EB1 association. To address this question, we produced a phosphomimetic version of tau with the serine 262 replaced by a glutamate residue (S262E-tau). The serine 262 is localized within the first tau repeat (R1) and has been shown to be phosphorylated in vivo in both physiological and pathological conditions (Seubert *et al.*, 1995). Phosphorylation at this site reduced microtubule-stabilizing properties of tau through intramolecular modifications (Trinczek *et al.*, 1995; Devred *et al.*, 2002; Kiris *et al.*, 2011). Here we showed that the phosphomimetic mutation of tau on S262 induced a twofold decrease in tau interaction with EB1 as detected by pull-down assays (50.1% ± 15.8 of S262E-tau bound to EB1 compared with tau, three independent experiments, mean ± SD; Figure 5A). We next performed end-tracking experiments of GFP-EB1 with either tau or S262E-tau. We first showed that S262E-tau alone was still able to stabilize microtubules by lowering catastrophes and promoting rescues, albeit less efficiently than tau (Figure 5D, compare third and fifth lines). In addition, with comparable tau:tubulin molar ratio used in the TIRF conditions (1:160), we observed a similar proportion of tau and S262E-tau bound to microtubules, as shown by cosedimentation assays performed on microtubules self-assembled with tau proteins (~1 tau or

(D) comets in the absence or presence of increasing concentrations of tau. ***$p < 0.001$; ****$p < 0.0001$; ns, nonsignificant; nonparametric Kruskal–Wallis ANOVA followed by post hoc Dunn's comparison (42, 37, and 48 microtubules for EB3, EB3 + 10 nM tau, and EB3 + 40 nM tau, respectively; 22, 40, and 30 microtubules for EB3-NL-LZ, EB3-NL-LZ + 10 nM tau, and EB3-NL-LZ + 40 nM tau, respectively). The p values were calculated in comparison to the conditions without tau. All error bars represent SD. a.u., arbitrary units.

	Growth rate (µm/min)	Shortening rate (µm/min)	Catastrophe frequency (events/min)	Rescue frequency (events/min)
Control	1.47 ± 0.28 $n = 62$	28.53 ± 12.6 $n = 44$	0.127 ± 0.019 $n = 44$	0
GFP-EB3 (10 nM)	1.94 ± 0.35 $n = 162$	28.17 ± 8.98 $n = 136$	0.440 ± 0.030 $n = 206$	0
tau (10 nM)	1.43 ± 0.63 $n = 35$	20.28 ± 12.96 $n = 7$	0.014 ± 0.005 $n = 7$	3.44 ± 1.3 $n = 7$
tau (40 nM)	1.83 ± 0.20 $n = 33$	37.41 $n = 1$	0.001 $n = 1$	10.01 $n = 1$
GFP-EB3 + 10 nM tau	1.49 ± 0.34 $n = 48$	26.90 ± 8.88 $n = 13$	0.024 ± 0.006 $n = 15$	2.57 ± 0.74 $n = 12$
GFP-EB3 + 40 nM tau	1.83 ± 0.41 $n = 51$	40.42 ± 14.64 $n = 2$	0.004 ± 0.002 $n = 2$	8.58 ± 6.06 $n = 2$
GFP-EB3-NL-LZ (10 nM)	2.12 ± 0.46 $n = 285$	25.99 ± 6.30 $n = 177$	0.450 ± 0.034 $n = 168$	0
GFP-EB3-NL-LZ + 10 nM tau	2.29 ± 0.77 $n = 105$	15.21 ± 5.90 $n = 92$	0.315 ± 0.032 $n = 92$	3.13 ± 0.32 $n = 92$
GFP-EB3-NL-LZ + 40 nM tau	1.83 ± 0.52 $n = 55$	20.48 ± 6.16 $n = 31$	0.056 ± 0.010 $n = 31$	2.07 ± 0.37 $n = 30$

Dynamic parameters were measured for microtubules assembled with tubulin (12 µM) in the absence or presence of the indicated proteins. The total times of measurements (growing and shrinkage phases) were 362.10, 497.24, 479.61, 513.44, 626.50, 457.13, 403.48, 321.11, and 565.12 min for tubulin alone, 10 nM GFP-EB3, 10 nM tau, 40 nM tau, 10 nM GFP-EB3 + 10 nM tau, 10 nM GFP-EB3 + 40 nM tau, 10 nM GFP-EB3-NL-LZ, 10 nM GFP-EB3-NL-LZ + 10 nM tau, and 10 nM GFP-EB3-NL-LZ + 40 nM tau, respectively. *n*, number of events measured for each condition. Values represent mean ± SD.

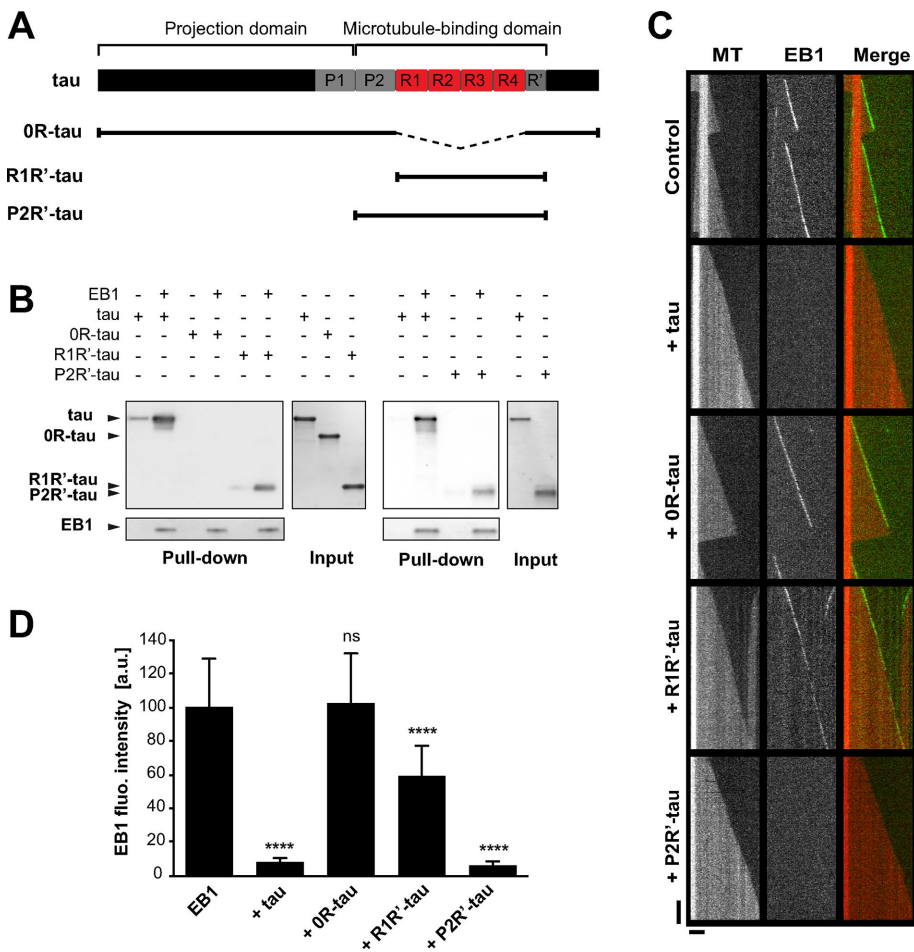TABLE 2: Effects of EB3, EB3-NL-LZ, and tau on microtubule dynamics.

FIGURE 4: EB1 interacts with tau microtubule-binding sites. (A) Schematic representation of full-length tau and the constructs used in this study. The N-terminal extremity and the proline-rich P1 region constitute the projection domain of tau. The microtubule-binding domain includes the second proline-rich P2 region, the tandem repeats (R1–R4). and the pseudorepeat motif (R′). (B) Pull-down assays of the indicated tau proteins with biotinylated-EB1. (C) Kymographs of individual microtubules growing with 75 nM GFP-EB1 in the absence (control) or presence of 75 nM indicated tau protein. MT, microtubule. (D) Fluorescence intensity of EB1 comets in the absence or in the presence of the indicated tau proteins. ****$p < 0.0001$; ns, nonsignificant; nonparametric Kruskal–Wallis ANOVA followed by post hoc Dunn's comparison (32, 27, 42, and 35 microtubules for EB1, EB1 + tau, EB1 + 0R-tau, and EB1 + R1R′-tau, respectively) and Mann–Whitney *U* test (30 and 39 microtubules for EB1 and EB1 + P2R′-tau, respectively). The *p* values were calculated in comparison to the condition without tau. All error bars represent SD. a.u., arbitrary units.

A

tau	+	+	-	-	+	-
S262E-tau	-	-	+	+	-	+
EB1	-	+	-	+	-	-

tau ▶

EB1 ▶

Pull-down   **Input**

B

C

MT EB1 Merge   MT EB1 Merge   MT EB1 Merge

Control   **+ tau**   **+ S262E-tau**

D

	Growth rate µm.min-1	Shortening rate µm.min-1	Catastrophe freq. events.min-1	Rescue freq. events.min-1
Control	1.27 ± 0.23 n = 46	29.54 ± 12.24 n = 40	0.145 ± 0.024 n = 34	0
EB1	1.24 ± 0.25 n = 137	24.15 ± 8.15 n = 122	0.256 ± 0.023 n = 114	0
tau	1.32 ± 0.16 n = 30	24.81 ± 7.26 n = 4	0.008 ± 0.004 n = 4	6.79 ± 3.35 n = 4
EB1 + tau	1.31 ± 0.13 n = 30	26.23 ± 7.98 n = 6	0.008 ± 0.035 n = 5	3.14 ± 1.40 n = 5
S262E-tau	1.48 ± 0.1 n = 59	21.06 ± 6.14 n = 15	0.015 ± 0.004 n = 13	1.08 ± 0.38 n = 8
EB1 + S262E-tau	1.15 ± 0.28 n = 109	17.05 ± 6.51 n = 80	0.074 ± 0.008 n = 76	0.96 ± 0.14 n = 47

FIGURE 5: S262E-tau interacts weakly with EB1 and does not inhibit EB1 tracking at microtubule ends. (A) Pull-down assays of tau and S262E-tau with biotinylated-EB1. One representative experiment. Quantifications indicate a decrease of 50.1% ± 15.8 of S262E-tau bound to EB1 compared with tau (three independent experiments, mean ± SD). (B) Quantification of fluorescence intensity of EB1 comets in the presence of tau or S262E-tau. *$p < 0.05$, ****$p < 0.0001$, nonparametric Kruskal–Wallis ANOVA followed by post hoc Dunn's comparison (37, 25, and 26 microtubules for EB1, EB1 + tau, and EB1 + S262E-tau, respectively). The p values were calculated in comparison to the condition without tau. Error bars represent SD. a.u., arbitrary units. (C) Kymographs of microtubules assembled with 75 nM GFP-EB1 in the absence (control) or presence of 75 nM of tau (+ tau) or S262E-tau (+ S262E-tau). Horizontal and vertical bars, 5 µm and 60 s, respectively. MT, microtubule. (D) Microtubule dynamics for tubulin alone (control) or in the presence of EB1, tau, S262E-tau, EB1 + tau, or EB1 + S262E-tau. The total times of measurements were 233.14, 444.28, 487.57, 567.19, 821.12, and 1014.26 min for tubulin alone, EB1, tau, EB1 + tau, S262E-tau, and EB1+S262E-tau, respectively. n, number of events measured for each condition. Values represent the mean ± SD.

S262E-tau molecule per 100 dimers of polymerized tubulin; Supplemental Figure S5). In the presence of both S262E-tau and GFP-EB1, we still observed GFP-EB1 comets at microtubule ends with a fluorescence intensity of ~71 a.u. compared with 100 a.u. for GFP-EB1 alone (Figure 5, B and C, right). Accordingly, microtubules underwent catastrophes and rescues due to the opposing microtubule-regulating activities of GFP-EB1 and S262E-tau (Figure 5D, sixth line).
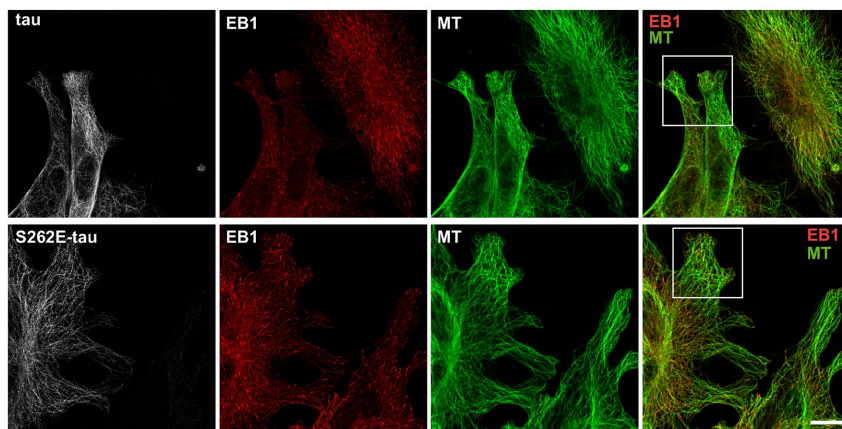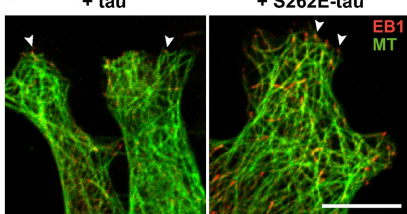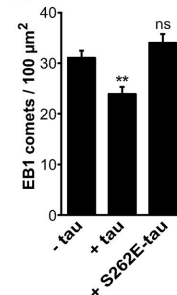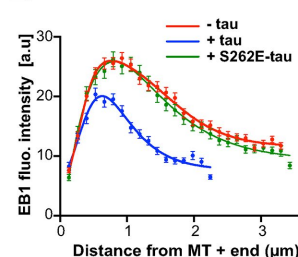
We next evaluated the effect of tau pseudophosphorylation on EB1 localization in fibroblasts expressing either tau or S262E-tau (Figure 6). In agreement with previous reports (Seubert *et al.*, 1995; Alonso *et al.*, 2010), S262E-tau was still able to bind to the microtubule lattice (Figure 6A, bottom). However, compared with the strong reduction of endogenous EB1 at microtubule ends in tau-transfected cells, S262E-tau expression did not induce any reduction of EB1 comets (Figure 6, A and B). Namely, the density (Figure 6C) and mean intensity (Figure 6D) of comets in S262E-tau transfected cells were similar to those in nontransfected cells. Furthermore, the average comet lengths were equivalent in S262E-tau-transfected cells (2.58 µm ± 0.04, 132 comets) and nontransfected cells (2.55 µm ± 0.03, 247 comets). Overall these data show that S262E-tau interacts less efficiently with EBs than tau and has little effect on EB comets at microtubule ends.

DISCUSSION

Structural MAPs primarily bind to and stabilize the microtubule lattice (Amos and Schlieper, 2005), whereas EB proteins preferentially accumulate at microtubule growing ends, where they modulate microtubule dynamics and microtubule interaction with cellular targets (Akhmanova and Steinmetz, 2010). Recent studies reported a role for structural MAPs in the regulation of EB localization in cells (Kapitein *et al.*, 2011; Tortosa *et al.*, 2013; Sayas *et al.*, 2015; Velot *et al.*, 2015); however, the underlying mechanisms remain poorly understood. Here we show that tau inhibits the microtubule end–tracking properties of EBs and that this inhibition is regulated by tau phosphorylation. The interplay between EBs and tau results in large changes in microtubule dynamics. In particular, blocking the function of EBs in the presence of equimolar concentration of tau induces stably growing microtubules. By contrast, restoring EB end-tracking properties at substoichiometric amounts of tau (or in the presence of tau phosphomutant) leads to dynamic polymers alternating between catastrophes (EB-destabilizing activity) and rescues (tau-stabilizing activity).

From our results, we propose that the formation of a soluble complex between tau and EBs negatively regulates EB tracking at microtubule ends (Figure 7). First, tau and EBs directly interact via the C-terminal region of EBs and the microtubule-binding sites of tau (Figures 3 and 4). Second, disruption of this complex by deletion of EB C-terminus (Figure 3) or phosphorylation of tau (Figure 5) causes the concomitant binding of tau and EBs to microtubules. Third, tau does not recruit EBs along microtubules (except in some cells expressing a high amount of tau; see later discussion), suggesting that EB-bound tau

FIGURE 6: S262E-tau does not inhibit endogenous EB1 localization at microtubule ends.
(A) Mouse embryonic fibroblasts were transfected with either pcDNA-tau (tau, top) or pcDNA-S262E-tau (S262E-tau, bottom) and stained for tau (gray), EB1 (red), and tubulin (MT, green). Right, merged images with EB1 and tubulin staining. Images include nontransfected and transfected cells in the same field. Bar, 10 μm. MT, microtubule. (B) Higher magnifications of cells transfected with pcDNA-tau (+tau) and pcDNA-S262E-tau (+S262E-tau). Arrowheads point to EB1 comets. Bar, 10 μm. (C) EB1 comet density normalized to the microtubule network surface (comet number/100 μm² of microtubule network) in lamellipodia of nontransfected cells (−tau) and cells transfected with tau (+tau) or S262E-tau (+S262E-tau). The histogram shows the mean ± SEM. **$p < 0.01$; ns, nonsignificant; nonparametric Kruskal–Wallis ANOVA followed by post hoc Dunn's comparison (74, 46, and 52 regions of interest for −tau, +tau, and +S262E-tau conditions, respectively). The p values were calculated in comparison to the condition without tau. (D) The fluorescence intensity of comets was quantified in nontransfected (−tau) and transfected cells (+tau and +S262E-tau) and plotted against distance from microtubule plus ends. Nonlinear regression curves fitting the mean fluorescence intensities ± SEM (247, 177, and 132 comets for −tau, +tau, and +S262E-tau cells, respectively). a.u., arbitrary units.

remains soluble (Figures 1E and 2). Moreover, the interaction between tau and EBs likely induces EB conformational changes, as tau binding to the C-terminal domain of EB1 results in fluorescence modifications of tryptophan residues that are located in the EB1 N-terminal region (Supplemental Figure S3). Tau could thus sequester EBs and/or affect EB conformation upon binding, thereby hampering +TIP localization to microtubule ends (Figure 7). The formation of such a complex might also affect tau properties, since EBs recognize the microtubule-binding sites of tau and should compete with tau/microtubule interaction. Indeed, the inhibitory activity of tau on catastrophes is impaired at substoichiometric amounts of tau compared with EB1, in agreement with the partial release of microtubule-bound tau by an excess of free EB1 (Figure 1 and Supplemental Figure S1). Strikingly, in the presence of equimolar concentrations of tau and EBs, tau still stabilizes microtubules (low catastrophe frequency associated with rescues), although it inhibits EB localization at MT ends (Figures 1, 3, and 5). We explain this behavior by the strong microtubule-stabilizing properties of tau: even very low quan-

tities of tau versus tubulin are able to suppress microtubule dynamics (Tables 1 and 2; Panda *et al.*, 1995, 2003). We therefore speculate that, in these conditions, the fraction of tau molecules not bound to EBs is sufficient to induce microtubule stabilization. Of note, the very fast turnover of tau onto microtubules that has been recently described in neurons is compatible with tau interaction with multiple partners (Janning *et al.*, 2014), which could also explain its capacities to both stabilize microtubules and bind EB proteins.

Alternatively, the association of tau with microtubules might indirectly influence EB localization by competing with the microtubule sites recognized by EBs and/or affecting the whole polymer structure. Accordingly, tau has been proposed to induce lattice structural modifications even at low tau:tubulin molar ratios, in the range of those used in the present study (Choi *et al.*, 2009). However, these hypotheses fail to explain the localization of EB3-NL-LZ at microtubule ends in the presence of tau (Figure 3), as well as the ability of EB1 to end-track microtubules copolymerized with S262E-tau, which still binds and stabilizes microtubules (Figures 5 and 6).

The inhibition of EB tracking at microtubule ends by tau in reconstitution assays is reminiscent of EB comet reduction in cells. Indeed, a decrease in EB localization to microtubule plus ends is observed in fibroblasts regardless of tau expression level (Figures 2 and 6) and also in neurons upon high tau expression (Sayas *et al.*, 2015). Intriguingly, high tau expression in both cell types (Supplemental Figure S1; Sayas *et al.*, 2015) leads to the relocation of EBs along tau-induced microtubule bundles, a phenomenon that we did not observe in purified cell-free systems. The presence of many MAPs and kinases in cells, as well as various

expression levels of tau during neuronal developmental stages and/or between subcellular compartments, may account for these differences. Furthermore, high tau concentrations have been proposed to trigger the formation of tau oligomers on the microtubule surface (Ackmann *et al.*, 2000); such tau oligomers with multiple microtubule- and EB-binding sites could induce the recruitment of EBs along microtubule bundles in cells expressing high amounts of tau, as recently proposed in neurons (Sayas *et al.*, 2015).

Of importance, the phosphomimetic mutation of tau within its microtubule-binding repeats strongly reduces tau/EB1 interaction. Furthermore, the S262E-tau mutant has only little effect on EB1 comets in both reconstituting assays and fibroblasts (Figures 5 and 6). In the presence of S262E-tau, EB1 can still bind to microtubule ends and exert its intrinsic catastrophe-promoting activity. Consequently, microtubules undergo both catastrophe and rescue events as a result of the combined activities of EB1 and S262E-tau (Figure 7C). Taken together, these data strongly suggest that the inhibitory effect of tau on EB localization to microtubule ends is

A EB1

B EB1 + tau

C EB1 + S262E-tau
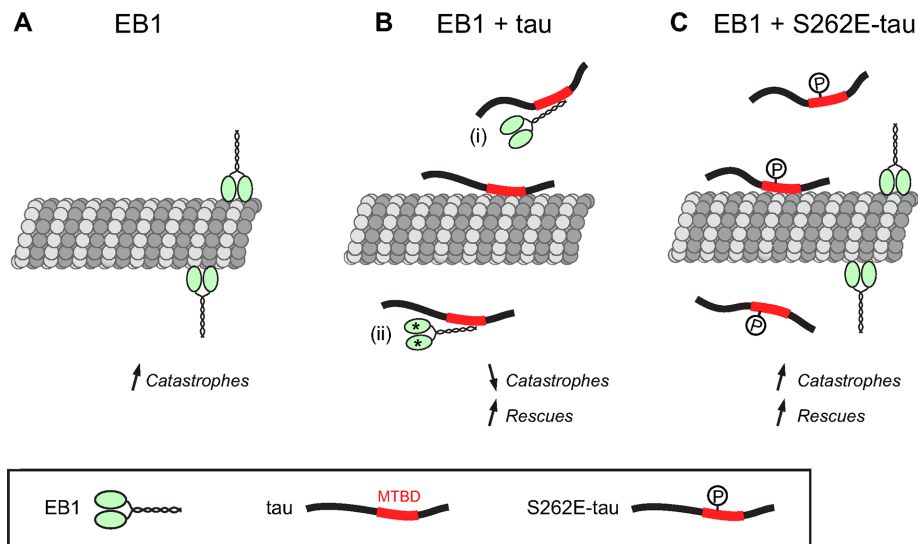
FIGURE 7: Model for the inhibitory activity of tau on EB tracking at microtubule ends. (A) In the absence of tau, EB1 binds to microtubule ends and exerts its intrinsic catastrophe-promoting activity. (B) The microtubule-binding domain (MTBD) of tau directly interacts with the C-terminal part of EB1. This interaction would hamper EB1 localization to microtubule ends through EB1 sequestration (i) and/or EB1 conformational changes (stars; ii). In these conditions, the catastrophe frequency decreases concomitantly with the apparition of rescues. (C) The phosphomimetic mutation S262E within tau MTBD impairs EB1/tau interaction and prevents tau-mediated inhibition of EB1 comets at microtubule ends. Microtubules are dynamic and undergo both catastrophes and rescues due to the opposing activities of EB1 and S262E-tau.

regulated by tau phosphorylation and open new perspectives on molecular dysfunctions possibly involved in tauopathies, such as Alzheimer's disease. Indeed, tau abnormal phosphorylation in these pathologies may have a direct effect on EB functions in neurons.

In conclusion, our work shows that tau directly antagonizes EB proteins through a phosphorylation-dependent mechanism, providing a new model for the regulation of EB end-tracking properties. Such a mechanism may represent an important way of regulation for microtubule dynamics and organization in neurons, where both types of protein are present and the importance of microtubules for the cell architecture is prominent.

MATERIALS AND METHODS
DNA constructs
We used the human tau isoform with one N-terminal insertion (N) and four microtubule-binding repeat (R) motifs (1N4R-tau, 412 amino acids; National Center for Biotechnology Information reference sequence NP_001116539.1) subcloned in the pDEST17 vector (kindly provided by N. Sergeant, Centre de Recherche Jean-Pierre Aubert, Lille, France). Deletion tau constructs were generated by a PCR-based strategy: 0R-tau, R1R′-tau, and P2R′-tau lack the Q244–K369 domain; the M1–Y168 and G372–L412 domains; and the M1–L243 and G372–L412 domains, respectively (amino acid numbers are given according to the longest 2N4R-tau isoform). Phosphomimetic tau mutant was generated by PCR using the QuikChange II XL site directed-mutagenesis kit (Agilent Technologies, Santa Clara, CA) to exchange the serine 262 by a glutamic acid residue (the S262 site refers to the amino acid sequence of the 2N4R-tau isoform). Mouse EB1 and human EB1-NL-LZ, GFP-EB1, GFP-EB3, and GFP-EB3-NL-LZ plasmids were kindly provided by M. Steinmetz (Paul Scherrer Institut, Villigen, Switzerland). EB1-NL-LZ and GFP-EB3-NL-LZ correspond to the N-terminal domains of EB1

(residues 1–189) and EB3 (residues 1–200) fused to the coiled-coil domain of GCN4 (Buey et al., 2011). The EB1-K100E/Q102E mutant (named EB1-KQ/EE in the text) was generated by PCR using the QuikChange II XL site directed-mutagenesis kit. The GFP-EB1 mutant lacking the last 20 amino acid residues (GFP-EB1-Δ-tail) was generated by a PCR-based strategy.

For pEGFP-tau, pcDNA-tau, and pcDNA-S262E-tau constructs, tau (1N4R isoform) or S262E-tau were PCR-amplified from the pD-EST constructs described and inserted into the pEGFP-C1 or pcDNA3.1 (+) plasmids using the In-Fusion HD Cloning kit (Clontech, Takara, Mountain View, CA).

Antibodies
For immunofluorescence, primary antibodies (Abs) were a mouse monoclonal Ab against the C-terminal part of EB1 (610534; BD Biosciences, San Jose, CA), a rabbit polyclonal Ab against human tau (A0024; Dako, Glostrup, Denmark), a rabbit polyclonal Ab against enhanced GFP (EGFP: AB3080, Millipore, Temecula, CA), and a rat monoclonal Ab against tyrosinated tubulin (clone YL1/2; Wehland and Willingham, 1983). Secondary antibodies were coupled to Alexa 488, Alexa 647 or Cyanine3 (Jackson Immuno-Research Laboratories, West Grove, PA).

Protein purification
Recombinant EB proteins were purified as described (Buey et al., 2011) and stored in K-BRB80 buffer (80 mM 1,4-piperazinediethanesulfonic acid, 1 mM ethylene glycol tetraacetic acid, 1 mM MgCl$_2$, 50 mM KCl, pH 6.8) and 20 mM Tris-HCl and 150 mM NaCl (pH 7.0), respectively. Histidine-tag recombinant tau proteins were purified using Talon metal affinity resin (Clontech) and further processed by size exclusion chromatography in BRB80 buffer. Tubulin was purified from bovine brain and fluorescently labeled with ATTO-565 (ATTO-Tech, Siegen, Germany) as previously described (Hyman et al., 1991). Protein concentrations refer to monomers for tau and EBs and to dimers for tubulin.

Pull-down assays
EB1 and EB1-NL-LZ proteins were biotinylated using the EZ-Link NHS-Chromogenic Biotinylation Kit (ThermoFisher Scientific, Waltham, MA). A 5-μg amount of biotinylated EB1 was incubated in 300 μl of PD-buffer (40 mM Tris-HCl, 50 mM NaCl, 0.05% Triton X-100, pH 7.0) with 5, 3.2, 1.9, and 2.1 μg of tau/S262E-tau, 0R-tau, R1R′-tau, and P2R′-tau, respectively (quantities of tau proteins were adjusted to obtain the same final molar concentrations). Samples were incubated for 15 min at 4°C before addition of streptavidin magnetic beads (ThermoFisher Scientific) and 60 min of incubation at 4°C. Streptavidin beads were washed in PD-buffer and resuspended in denaturing Laemmli sample buffer. Tau proteins recovered with beads were detected by Western blot using a polyclonal anti-tau primary antibody (dilution 1:10,000; Dako) and a horseradish peroxidase–conjugated anti-rabbit secondary antibody (1:2000; ThermoFisher Scientific), followed by enhanced chemiluminescence revelation. EB1 bound to

the beads was visualized on Coomassie-stained gels. Differences in tau and S262E-tau interaction with EB1 were quantified on immunoblots using ImageJ software (Schneider *et al.*, 2012). For pull-down experiments comparing tau interaction with EB1-NL-LZ and EB1, EB proteins associated with magnetic beads were detected on Western blot using an anti-biotin antibody (1:2000) and anti-mouse EB1 (1:2000).

Microtubules/tau cosedimentation assays

To compare the proportion of tau and S262E-tau bound to microtubules, microtubules were self-assembled in the presence of tau or S262E-tau proteins in K-BRB80 buffer supplemented with 1 mM GTP at 32°C and at a tau:tubulin molar ratio of 1:160 (40 µM tubulin dimers with 0.25 µM tau or S262E-tau). After 30 min of incubation, microtubules were centrifuged for 30 min at 230,000 × g and analyzed by SDS–PAGE. The amounts of tau bound to microtubules and of total polymerized tubulin were determined on immunoblots and Coomassie-stained gels, respectively. In the absence of microtubules, no tau was detected in the pellet.

TIRF microscopy, image analysis, and microtubule dynamics

Perfusion chambers were functionalized with silane-PEG-biotin (Laysanbio, Arab, AL) coverslips and silane-PEG (Creative PEGwork, Chapel Hill, NC) glass slides as described (Elie *et al.*, 2015). The flow cell was perfused with NeutrAvidin (25 µg/ml in 1% bovine serum albumin [BSA]; ThermoFisher Scientific), PLL-g-PEG (2 kDa, 0.1 mg/ml in 10 mM 4-(2-hydroxyethyl)-1-piperazineethanesulfonic acid, pH 7.4; Jenkem, Plano, TX), 1% BSA in BRB80, and GMPCPP-stabilized, ATTO-565–labeled microtubule seeds. Microtubules assembly was initiated with 12 µM tubulin (containing 30% ATTO 565–labeled tubulin) in the presence of various combinations of GFP-EBs and tau proteins in TIRF assay buffer (4 mM dithiothreitol, 1% BSA, 50 mM KCl, 1 mg/ml glucose, 70 µg/ml catalase, 580 µg/ml glucose oxidase, and 0.1% methylcellulose [4000 cP; Sigma-Aldrich, St. Louis, MO] in BRB80). For experiments with GFP-EB1, final concentrations of GFP-EB1 (monomers) and tau proteins (tau, R1R′-tau, and P2R′-tau) were fixed to 75 nM. The concentration of 0R-tau was increased to 500 nM since the deletion of the repeats drastically inhibits its microtubule-stabilizing properties (Trinczek *et al.*, 1995). For experiments with EB3-GFP and GFP-EB3-NL-LZ, we decreased the GFP-EB concentration (monomers) to 10 nM to avoid extensive microtubule lattice binding of GFP-EB3-NL-LZ (Buey *et al.*, 2011). Tau concentrations were fixed to 10 and 40 nM. Dual-color time-lapse imaging was performed on an inverted Eclipse Ti (Nikon, Melville, NY) microscope with an Apochromat 60×/1.49 numerical aperture (NA) oil immersion objective (Nikon) equipped with an ilas2 TIRF system (Roper Scientific, Evry, France) and a cooled charged-coupled device camera (EMCCD Evolve 512; Photometrics, Tucson, AZ) and was controlled by the MetaMorph 7.7.5 software (Molecular Devices, Sunnyvale, CA). For excitation, we used 491- and 561-nm lasers and performed time-lapse imaging at 1 frame per 2 s with an 80-ms exposure time.

All image analysis was done with ImageJ software and a homemade KymoTool. Comet fluorescence intensities were measured on the frames of the first 90 s of time-lapse movies using kymographs with background subtraction (Maurer *et al.*, 2011). The maximum fluorescence intensity at microtubule growing ends was measured in the green channel with a 5-pixel-wide line. Comparisons of fluorescence intensities with and without tau proteins were calculated from experiments performed with the same acquisition

setup and laser intensity. Microtubule dynamic parameters were determined on kymographs using ImageJ software. Growing and shortening rates of microtubules were calculated from the slopes of individual growth or shrinkage phases. The catastrophe and rescue frequencies were determined by dividing the total number of events by the time spent in growing and shrinking phases, respectively. For these two parameters, the SD corresponds to the rescue (or catastrophe) frequency divided by $\sqrt{n}$, where n is the number of the total observed events, assuming a Poisson distribution (Walker *et al.*, 1988).

Cell culture, transfection, immunofluorescence, and image quantification

Mouse embryonic fibroblasts were prepared from embryonic day 14.5 embryos following standard procedures and cultured in DMEM and 1 g/l glucose with 10% fetal bovine serum. Transient transfections were carried out with 3 µg of plasmid DNA per 35-mm dish using Lipofectamine LTX reagent (ThermoFisher Scientific) and according to the manufacturer's protocol. After 24 h of transfection, cells were fixed by a 10-min incubation in methanol at −20°C. Immunofluorescence was performed using standard procedures. Fluorescence images were acquired with a Zeiss LSM 710 confocal microscope using a 63× oil-immersion objective (NA 1.4) and ZEN 2010 software (Carl Zeiss MicroImaging, Oberkochen, Germany). Acquisition settings were identical between all images for one set of experiments to allow quantifications and comparisons.

Quantification of EB1 comet densities was performed on regions of interest drawn around cell lamellipodia using a homemade macro on ImageJ software (Schneider *et al.*, 2012). First, in order to calculate the microtubule network surface, a binary image was produced by applying a bandpass filter and automatic thresholding to the microtubule channel. Second, to detect comets, the same procedure was applied to the EB1 channel. Comets located onto microtubules were recovered by multiplying the two binary images. The comet density was obtained by dividing the number of comets by the microtubule network surface.

Length and fluorescence intensity of comets were quantified by drawing a line scan over a comet at microtubule end. At least 20 comets per cell were quantified, and the mean intensity was calculated by subtracting the background for each cell. Comet fluorescence intensities for at least five cells per condition were averaged and plotted against the distance from the microtubule plus end.

Statistics

All statistical analyses were done using Prism 6 (GraphPad Software, La Jolla, CA).

REFERENCES

Ackmann M, Wiech H, Mandelkow E (2000). Nonsaturable binding indicates clustering of tau on the microtubule surface in a paired helical filament-like conformation. J Biol Chem 275, 30335–30343.

Akhmanova A, Steinmetz MO (2010). Microtubule +TIPs at a glance. J Cell Sci 123, 3415–3419.

Alonso AD, Di Clerico J, Li B, Corbo CP, Alaniz ME, Grundke-Iqbal I, Iqbal K (2010). Phosphorylation of tau at Thr212, Thr231, and Ser262 combined causes neurodegeneration. J Biol Chem 285, 30851–30860.

Amos LA, Schlieper D (2005). Microtubules and maps. Adv Protein Chem 71, 257–298.

Bieling P, Laan L, Schek H, Munteanu EL, Sandblad L, Dogterom M, Brunner D, Surrey T (2007). Reconstitution of a microtubule plus-end tracking system in vitro. Nature 450, 1100–1105.

Buee L, Bussiere T, Buee-Scherrer V, Delacourte A, Hof PR (2000). Tau protein isoforms, phosphorylation and role in neurodegenerative disorders. Brain Res Brain Res Rev 33, 95–130.

Buey RM, Mohan R, Leslie K, Walzthoeni T, Missimer JH, Menzel A, Bjelic S, Bargsten K, Grigoriev I, Smal I, et al. (2011). Insights into EB1 structure and the role of its C-terminal domain for discriminating microtubule tips from the lattice. Mol Biol Cell 22, 2912–2923.

Choi MC, Raviv U, Miller HP, Gaylord MR, Kiris E, Ventimiglia D, Needleman DJ, Kim MW, Wilson L, Feinstein SC, et al. (2009). Human microtubule-associated-protein tau regulates the number of protofilaments in microtubules: a synchrotron x-ray scattering study. Biophys J 97, 519–527.

De Groot CO, Jelesarov I, Damberger FF, Bjelic S, Scharer MA, Bhavesh NS, Grigoriev I, Buey RM, Wuthrich K, Capitani G, et al. (2010). Molecular insights into mammalian end-binding protein heterodimerization. J Biol Chem 285, 5802–5814.

Desai A, Mitchison TJ (1997). Microtubule polymerization dynamics. Annu Rev Cell Dev Biol 13, 83–117.

Devred F, Douillard S, Briand C, Peyrot V (2002). First tau repeat domain binding to growing and taxol-stabilized microtubules, and serine 262 residue phosphorylation. FEBS Lett 523, 247–251.

Dixit R, Barnett B, Lazarus JE, Tokito M, Goldman YE, Holzbaur EL (2009). Microtubule plus-end tracking by CLIP-170 requires EB1. Proc Natl Acad Sci USA 106, 492–497.

Elie A, Prezel E, Guerin C, Denarier E, Ramirez-Rios S, Serre L, Andrieux A, Fourest-Lieuvin A, Blanchoin L, Arnal I (2015). Tau co-organizes dynamic microtubule and actin networks. Sci Rep 5, 9964.

Galjart N (2010). Plus-end-tracking proteins and their interactions at microtubule ends. Curr Biol 20, R528–R537.

Hayashi I, Ikura M (2003). Crystal structure of the amino-terminal microtubule-binding domain of end-binding protein 1 (EB1). J Biol Chem 278, 36430–36434.

Honnappa S, Gouveia SM, Weisbrich A, Damberger FF, Bhavesh NS, Jawhari H, Grigoriev I, van Rijssel FJ, Buey RM, Lawera A, et al. (2009). An EB1-binding motif acts as a microtubule tip localization signal. Cell 138, 366–376.

Honnappa S, John CM, Kostrewa D, Winkler FK, Steinmetz MO (2005). Structural insights into the EB1-APC interaction. EMBO J 24, 261–269.

Hyman A, Drechsel D, Kellogg D, Salser S, Sawin K, Steffen P, Wordeman L, Mitchison T (1991). Preparation of modified tubulins. Methods Enzymol 196, 478–485.

Janning D, Igaev M, Sundermann F, Bruhmann J, Beutel O, Heinisch JJ, Bakota L, Piehler J, Junge W, Brandt R (2014). Single-molecule tracking of tau reveals fast kiss-and-hop interaction with microtubules in living neurons. Mol Biol Cell 25, 3541–3551.

Kapitein LC, Yau KW, Gouveia SM, van der Zwan WA, Wulf PS, Keijzer N, Demmers J, Jaworski J, Akhmanova A, Hoogenraad CC (2011). NMDA receptor activation suppresses microtubule growth and spine entry. J Neurosci 31, 8194–8209.

Kiris E, Ventimiglia D, Sargin ME, Gaylord MR, Altinok A, Rose K, Manjunath BS, Jordan MA, Wilson L, Feinstein SC (2011). Combinatorial Tau pseudophosphorylation: markedly different regulatory effects on microtubule assembly and dynamic instability than the sum of the individual parts. J Biol Chem 286, 14257–14270.

Komarova Y, De Groot CO, Grigoriev I, Gouveia SM, Munteanu EL, Schober JM, Honnappa S, Buey RM, Hoogenraad CC, Dogterom M, et al. (2009). Mammalian end binding proteins control persistent microtubule growth. J Cell Biol 184, 691–706.

Maurer SP, Bieling P, Cope J, Hoenger A, Surrey T (2011). GTPgammaS microtubules mimic the growing microtubule end structure recognized by end-binding proteins (EBs). Proc Natl Acad Sci USA 108, 3988–3993.

Maurer SP, Fourniol FJ, Bohner G, Moores CA, Surrey T (2012). EBs recognize a nucleotide-dependent structural cap at growing microtubule ends. Cell 149, 371–382.

Mitchison T, Kirschner M (1984). Microtubule assembly nucleated by isolated centrosomes. Nature 312, 232–237.

Mukrasch MD, Bibow S, Korukottu J, Jeganathan S, Biernat J, Griesinger C, Mandelkow E, Zweckstetter M (2009). Structural polymorphism of 441-residue tau at single residue resolution. PLoS Biol 7, e34.

Mukrasch MD, von Bergen M, Biernat J, Fischer D, Griesinger C, Mandelkow E, Zweckstetter M (2007). The "jaws" of the tau-microtubule interaction. J Biol Chem 282, 12230–12239.

Panda D, Daijo JE, Jordan MA, Wilson L (1995). Kinetic stabilization of microtubule dynamics at steady state in vitro by substoichiometric concentrations of tubulin-colchicine complex. Biochemistry 34, 9921–9929.

Panda D, Samuel JC, Massie M, Feinstein SC, Wilson L (2003). Differential regulation of microtubule dynamics by three- and four-repeat tau: implications for the onset of neurodegenerative disease. Proc Natl Acad Sci USA 100, 9548–9553.

Sayas CL, Avila J (2014). Regulation of EB1/3 proteins by classical MAPs in neurons. Bioarchitecture 4, 1–5.

Sayas CL, Tortosa E, Bollati F, Ramirez-Rios S, Arnal I, Avila J (2015). Tau regulates the localization and function of End-binding proteins 1 and 3 in developing neuronal cells. J Neurochem 133, 653–667.

Schneider CA, Rasband WS, Eliceiri KW (2012). NIH Image to ImageJ: 25 years of image analysis. Nat Methods 9, 671–675.

Seubert P, Mawal-Dewan M, Barbour R, Jakes R, Goedert M, Johnson GV, Litersky JM, Schenk D, Lieberburg I, Trojanowski JQ, et al. (1995). Detection of phosphorylated Ser262 in fetal tau, adult tau, and paired helical filament tau. J Biol Chem 270, 18917–18922.

Skube SB, Chaverri JM, Goodson HV (2010). Effect of GFP tags on the localization of EB1 and EB1 fragments in vivo. Cytoskeleton 67, 1–12.

Slep KC, Rogers SL, Elliott SL, Ohkura H, Kolodziej PA, Vale RD (2005). Structural determinants for EB1-mediated recruitment of APC and spectraplakins to the microtubule plus end. J Cell Biol 168, 587–598.

Tortosa E, Galjart N, Avila J, Sayas CL (2013). MAP1B regulates microtubule dynamics by sequestering EB1/3 in the cytosol of developing neuronal cells. EMBO J 32, 1293–1306.

Trinczek B, Biernat J, Baumann K, Mandelkow EM, Mandelkow E (1995). Domains of tau protein, differential phosphorylation, and dynamic instability of microtubules. Mol Biol Cell 6, 1887–1902.

Velot L, Molina A, Rodrigues-Ferreira S, Nehlig A, Bouchet BP, Morel M, Leconte L, Serre L, Arnal I, Braguer D, et al. (2015). Negative regulation of EB1 turnover at microtubule plus ends by interaction with microtubule-associated protein ATIP3. Oncotarget 6, 43557–43570.

Vitre B, Coquelle FM, Heichette C, Garnier C, Chretien D, Arnal I (2008). EB1 regulates microtubule dynamics and tubulin sheet closure in vitro. Nat Cell Biol 10, 415–421.

Walker RA, O'Brien ET, Pryer NK, Soboeiro MF, Voter WA, Erickson HP, Salmon ED (1988). Dynamic instability of individual microtubules analyzed by video light microscopy: rate constant and transition frequencies. J Cell Biol 107, 1437–1448.

Wehland J, Willingham MC (1983). A rat monoclonal antibody reacting specifically with the tyrosylated form of alpha-tubulin. II. Effects on cell movement, organization of microtubules, and intermediate filaments, and arrangement of Golgi elements. J Cell Biol 97, 1476–1490.

Zanic M, Stear JH, Hyman AA, Howard J (2009). EB1 recognizes the nucleotide state of tubulin in the microtubule lattice. PLoS One 4, e7585.

Zanic M, Widlund PO, Hyman AA, Howard J (2013). Synergy between XMAP215 and EB1 increases microtubule growth rates to physiological levels. Nat Cell Biol 15, 688–693.

Zhang R, Alushin GM, Brown A, Nogales E (2015). Mechanistic origin of microtubule dynamic instability and its modulation by EB proteins. Cell 162, 849–859.

Zimniak T, Stengl K, Mechtler K, Westermann S (2009). Phosphoregulation of the budding yeast EB1 homologue Bim1p by Aurora/Ipl1p. J Cell Biol 186, 379–391.

Supplemental Materials
Molecular Biology of the Cell

Ramirez-Rios et al.

Tau antagonizes EB tracking at microtubule ends through a phosphorylation-dependent mechanism

Sacnicte Ramirez-Rios, Eric Denarier, Eléa Prezel, Angélique Vinit, Virginie Stoppin-Mellet, François Devred, Pascale Barbier, Vincent Peyrot, Carmen Laura Sayas, Jesus Avila, Leticia Peris, Annie Andrieux, Laurence Serre, Anne Fourest-Lieuvin and Isabelle Arnal

Supplemental Materials:

- Supplemental Figures
- Supplemental Movie Legends
- Supplemental Materials and Methods
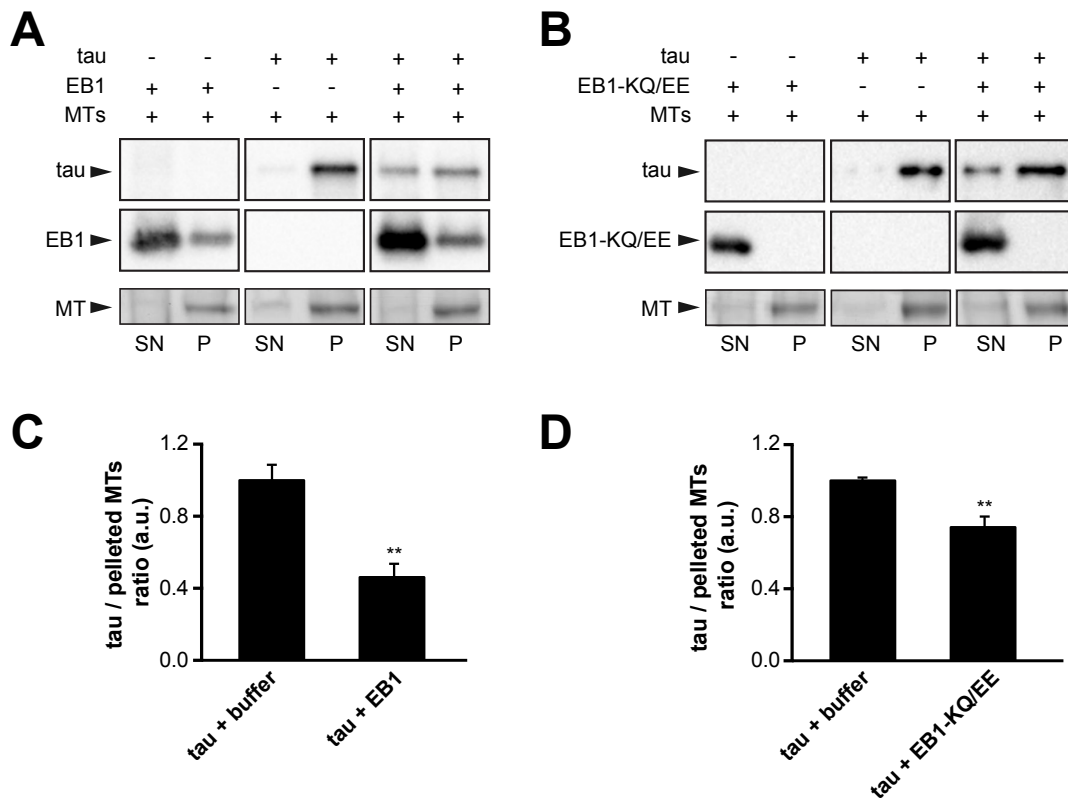
Figure S1. EB1 affects microtubule-binding properties of tau. (A) A two-step co-sedimentation assay was performed to analyse the effect of EB1 on tau-bound microtubules. Taxol-stabilized microtubules (2 μM) were incubated with tau (1μM), centrifuged to remove unbound tau and resuspended in either buffer alone (middle panel) or in the presence of 20 μM EB1 (right panel). Microtubules were then centrifuged again and the relative amounts of tau recovered with pelleted microtubules were quantified. The left panel shows the control experiment without tau. MT, microtubule; P, pellet; SN, supernatant. (B) Similar two-step co-sedimentation assay as in (A) performed with EB1-KQ/EE, a mutated form of EB1 exhibiting impaired microtubule-binding properties. (C) and (D) Quantifications of the ratios of tau to microtubules recovered in the final pellets after incubation with buffer alone (tau + buffer) or with either EB1 (tau + EB1) or EB1-KQ/EE (tau + EB1-KQ/EE). **$p<0.01$, non-parametric Mann-Whitney U test comparison (n = 5 independent experiments). Errors bars represent SEM.
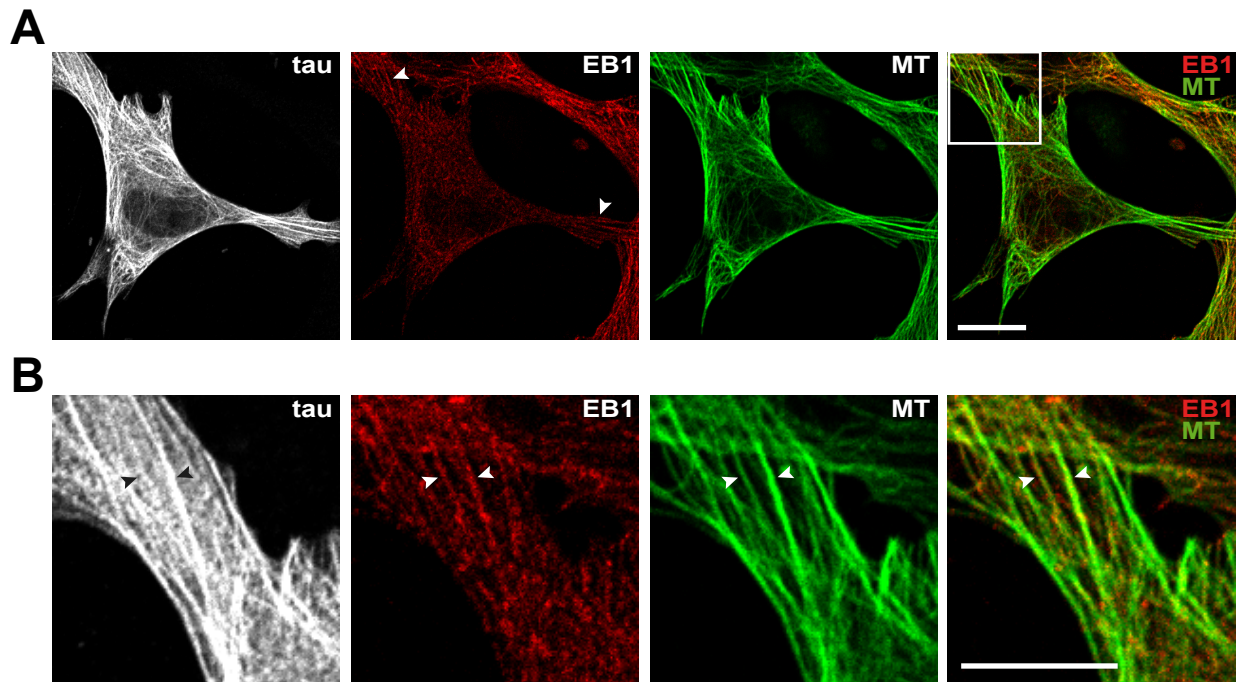
Figure S2. EB1 relocates along tau-induced microtubule bundles in fibroblasts upon high tau expression levels. (A) Mouse embryonic fibroblasts were transfected with pEGFP-tau and stained for EGFP (tau, in gray), EB1 (red) and tubulin (MT, green). A merged image with EB1 and microtubule staining is shown on the right. Images include transfected and non-transfected cells in the same field. Arrowheads point to EB1 relocated along microtubule bundles. Scale bar, 10 μm. (B) Higher magnification of the tau-induced microtubule bundles in the transfected cell. Arrowheads point to microtubules bundles along which EB1 is relocated. Scale bar, 10 μm.
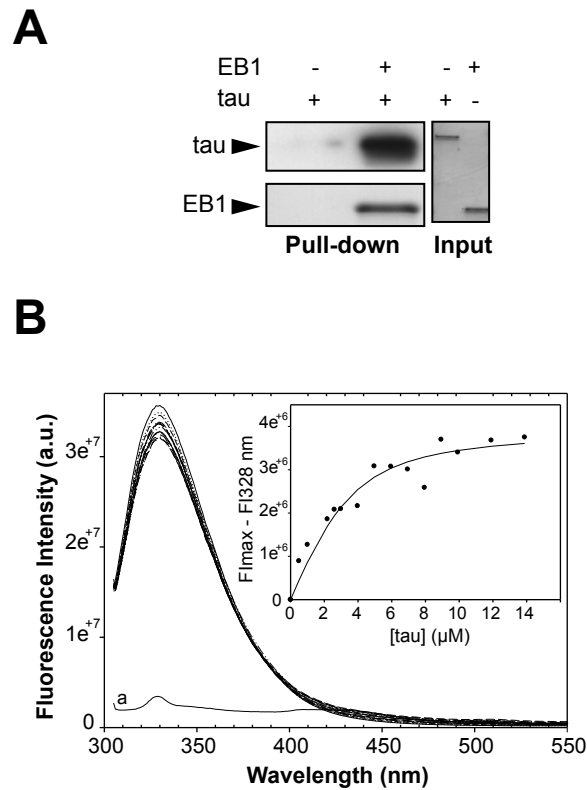
Figure S3. EB1 directly interacts with tau. (A) Pull-down assay of tau and biotinylated-EB1. (B) Representative plot of EB1/tau interaction monitored by fluorescence. EB1 fluorescence emission quenching is followed upon tau addition (λ exc = 295 nm). EB1 (6.3 µM) in BRB80 pH 6.74, 50 mM KCl, was mixed at 25 °C with increasing tau concentrations from 0 (upper spectrum) to 14 µM (lower spectrum). The bottom curve (a) represents the fluorescence spectrum of tau alone (9 µM), which is almost flat due to the absence of tryptophan in the protein. The graph (inset) shows the resulting titration plot as Fmax-F in function of total tau concentration from which we found a value of Kd about 1.7 ± 1.1 µM. Circle symbols indicate the experimental points (collected at 328 nm), and the solid line is the fitting curve obtained as described in Supplemental Materials and Methods).
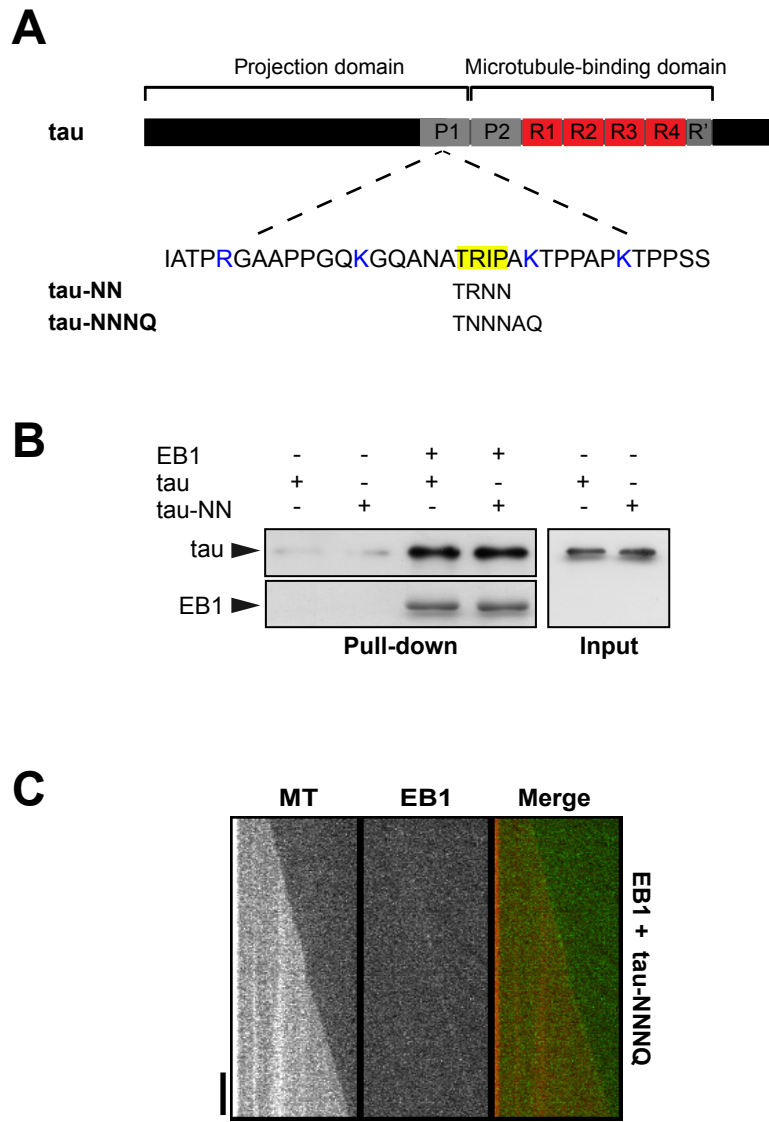
Figure S4. Mutations of the putative SxIP EB1-binding motif of tau does not affect tau/EB1 interaction and does not prevent tau-dependent inhibition of EB1 end-tracking. (A) Tau contains in its proline-rich region P1 a linear Ser-x-Ile-Pro (SxIP) motif (highlighted in yellow) flanking by basic residues (highlighted in blue). This motif shares the characteristic features of EB1-binding sites found on several EBs partners (Honnappa *et al.*, 2009). The replacement of IP or flanking basic residues by Asn (N) or Gln (Q) has been shown to abolish the interaction between EB1 and proteins that contain this motif (Honnappa *et al.*, 2009). (B) Pull-down assay of tau and tau-NN (mutated on IP residues) with biotinylated-EB1. (C) Kymographs of microtubules assembled in the presence of EB1 and tau NNNQ (mutated on xIP and adjacent lysine). Horizontal and vertical scale bars, 5 µm and 60 s.
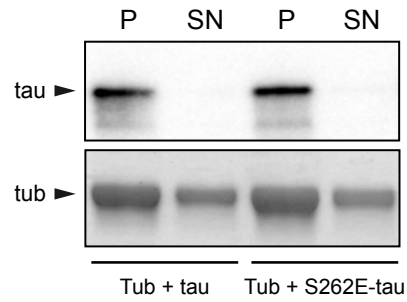
Figure S5. Comparison of the microtubule-binding properties of tau and S262E-tau by co-sedimentation assays. Microtubules were self-assembled in the presence of either tau or S262E-tau under similar tau:tubulin ratio used in TIRF conditions (1:160), before being centrifuged. Quantifications indicate that similar amounts of tau and S262E-tau bind to microtubules: 0.75 ± 0.066 and 0.83 ± 0.12 molecules bound to 100 molecules of polymerized tubulin dimers respectively (three independent experiments, mean $\pm$ SD). P, pellet; SN, supernatant; tub, tubulin.

Supplemental Movie Legends

Movie S1. Tau inhibits microtubule end tracking of EB1.
GFP-EB1 (75 nM) tracks growing microtubule ends and promotes catastrophe events (upper panels). Addition of equimolar concentration of tau (75 nM) inhibits the plus-end tracking of GFP-EB1 (lower panels) leading to persistently growing microtubules. Scale bar, 10 μm.

Movie S2. Increasing concentrations of tau reduce GFP-EB3 end tracking.
GFP-EB3 (10 nM) tracks growing ends of microtubules (upper right). Increasing concentration of tau (10 nM middle, and 40 nM lower panel) strongly reduced GFP-EB3 end tracking. Scale bar, 10 μm.

Movie S3. C-terminal deletion of EB3 allows recovering of microtubule end tracking in the presence of tau.
GFP-EB3-NL-LZ (10 nM) tracks growing ends of microtubules in the absence (upper panels) or in the presence of increasing concentrations of tau (10 and 40 nM, middle and lower panels). Scale bar, 10 μm.

Supplemental Materials and Methods

Co-sedimentation assay of taxol-stabilized microtubules, tau and EB1

Taxol-stabilized microtubules were prepared by incubating 70 μM tubulin at 36°C in BRB80 buffer supplemented with 1 mM GTP. Taxol (70 μM final) was then added and microtubules were further incubated for 30 minutes. Microtubules were then centrifuged for 5 minutes at 230,000 g and resuspended in BRB80 buffer.

For co-sedimentation assays, taxol-stabilized microtubules (2 μM) were incubated at room temperature with tau (1 μM) in K-BRB80 and centrifuged for 30 minutes at 230,000 x g to remove unbound tau. Microtubules were resuspended in buffer alone (K-BRB80) or in the presence of 20 μM EB1 or EB1-KQ/EE. After 30 minutes incubation, the mixtures were centrifuged again on a 50 % sucrose cushion for 45 minutes at 230,000 x g. Pellets and supernatants were analysed by SDS-PAGE and immunoblots to quantify the amounts of microtubules and tau, respectively. In the absence of microtubules, neither tau nor EB1 (wild-type and mutated EB1-KQ/EE) was detected in the pellet.

Fluorescence spectroscopy

Fluorescence experiments were done in a Perkin Elmer spectrofluorimeter. When EB1 were excited at 295 nm, the tryptophan residues show fluorescence maximum emission at 328 nm. In presence of different concentrations of tau (that does not have tryptophan residues), this emission is quenched due to the complex formation. EB1 (6 µM) was titrated using a 500 µM Tau solution. We used thermostated cuvettes (1 x 0.2 cm) at 25°C and put the smaller light path toward the excitation direction to give no appreciable inner filter effect (OD < 0.05). The fluorescence intensities (F) obtained at 328 nm for the different concentrations of tau was subtracted from the fluorescence intensity of EB1 alone (Fmax) and plotted versus the total tau concentration. The data were then were fitted to the saturation curve equation by means of nonlinear least-squares regression analysis using:

$$\text{Fmax} - \text{F} = \frac{\text{Fsat} \times [\text{tau}]\text{f}}{\text{Kd} + [\text{tau}]\text{f}}$$

Where Fsat is the fluorescence signal at the saturation, [tau]f is the free tau concentration and Kd is the dissociation equilibrium constant. Concentrations and binding parameters were determined as previously described [36]. Briefly, we used the equation:

[tau]b

$$= \frac{1}{2} \left\{ ([tau]_0 + n\,[EB1]_0 + Kd) - \sqrt{([tau]_0 + n\,[EB1]_0 + Kd)^2 - 4n\,[tau]_0[EB1]_0} \right\}$$

where $[tau]_0$ and $[EB1]_0$ are the total tau and EB1 concentrations, respectively, [tau]b the bound tau concentration, and n the apparent stoichiometry ([tau]/[EB1]) that was fixed to 0.5 to obtain the best fit.